受入
86-11-188
高工研図書室

UNIVERSITÄT BONN
Physikalisches Institut

Diffraction Dissociation at the CERN Pulsed Collider at c.m. energies of 900 and 200 GeV

UA5 Collaboration
Bonn[1], Brussels[2], Cambridge[3], CERN[4], Stockholm[5]

R.E.Ansorge[3], B. Åsman[5], C.N.Booth[4], L.Burow[1], P.Carlson[5], R.S.DeWolf [3], A.Drees[1], B.Eckart[1], G.Ekspong[5], I.Evangelou[4#], C.Fuglesang[5], J.Gaudean[2], C.Geich-Gimbel[1], B.Holl[1], R.Hospes[1], K.Jon-And[5], D.P.Johnson[2], F.Lotse[5], N.Manthos[4#], D.J.Munday[3], J.E.V.Ovens[3], W.Pelzer[1], J.G.Rushbrooke[3], H.Schmickler[1], F.Triantis[4#], L.Van hamme[2], C.Walck[5], C.P.Ward[3], D.R.Ward[3], C.J.S.Webber[3], T.O.White[3], G.Wilquet[2] and N.Yamdagni[5]

Abstract: Cross-sections for diffractive particle production and pseudorapidity distributions of the decay products of diffractive states are presented. The data were obtained with the UA5 streamer chamber detector at the CERN $p\bar{p}$ Collider operated in a new pulsed mode yielding $p\bar{p}$ interactions at c.m. energies of 900 and 200 GeV. Data recorded with a special trigger designed to select a sample of events enriched in single-diffractive interactions clearly favour a p_t-limited fragmentation of diffractive states. The cross-section for single-diffractive particle production σ_{SD} was found to be $7.8 \pm 0.5 \pm 1.1$ mb at 900 GeV and $4.8 \pm 0.5 \pm 0.8$ mb at 200 GeV (first error statistical, second systematic). From the pseudorapidity distribution of diffractive states we deduce the average number of charged particles to be 6.5 ± 1.0 at 900 GeV and 4.1 ± 1.1 at 200 GeV. Furthermore we report on our estimates for the cross-section of double-diffractive particle production at both Collider energies.

To be submitted to Zeitschrift für Physik C

[1] Physikalisches Institut der Universität Bonn, Germany
[2] Inter-University Institute for High Energies (ULB-VUB), Brussels, Belgium
[3] Cavendish Laboratory, Department of Physics, Cambridge University, UK
[4] CERN, Geneva, Switzerland
[5] Institute of Physics, University of Stockholm, Sweden
[#] Also at the University of Ioannina, Greece.

Post address:
Nussallee 12
D-5300 Bonn 1
W-Germany

BONN - HE-86-19
Bonn University
July 1986
ISSN-0172-8733

I. Introduction

The existence of highly inelastic excitations of interacting particles with diffractive like signatures (sharp forward peak, no quantum number exchanges) was predicted in 1956, 1960 [1,2]. Inelastic diffraction was viewed as a process which puts virtual hadronic states on the mass shell, the mass M of such states only being limited by the coherence condition $M^2/s \leq (m_p \cdot R)^{-1}$, where $\sqrt{s}$ is the c.m. energy of the collision and R is the interaction radius. Taking $R = m_\pi^{-1}$ leads to $M^2/s \leq m_\pi/m_p \simeq 0.15$. In common with most previous experiments we shall restrict ourselves to the region $M^2/s \leq 0.05$, where the diffractive peak is clearly seen.

From the above limit it is clear that a separation and detailed study of high mass diffractive events has become possible due to the significant increase of available collision energy at current accelerator experiments. Experimental information concerning the inclusive reaction pp $\rightarrow$ pX at lower energies, reviewed in [3,4], established the existence of a production mechanism sharply peaking near $x_F = 1$, ($x_F = 2p_L/\sqrt{s}$ is the ratio of the momentum of the recoiling proton in the above reaction to the incident beam momentum). Approximate M^2/s scaling of the cross-section was observed with a form $d\sigma/(dM^2/s) \sim (M^2/s)^{-1}$, consistent with the expectations of triple-Regge ideas [5].[1] A basic question is still the behaviour of the total cross-section for this process as a function of the c.m. energy of the initial collision. A comparison of existing data and our new data may help to distinguish between different model predictions, despite uncertainties resulting from the fact that different analysis methods had to be used over the wide energy span to separate diffractive events. Within the perturbative Reggeon Calculus [6,7,8], the Pomeron-Photon Analogy [9] and the triple-Regge approach [5] a rise of the single-diffractive cross-section with energy is predicted, whereas for example in the quark-glue model [10] a cross-section of about 6 mb is calculated for the ISR energy range and only a slow logarithmic rise of the single-diffractive cross-section seems to be possible if one extends this model to higher energies.

The UA5 collaboration has carried out experiments at the CERN $p\bar{p}$ Collider in 1981 and 1982 at $\sqrt{s} = 546$ GeV. This collision energy was mainly limited by the maximum power dissipation of the SPS ring magnets. Following a proposal made in 1982 [11] it is possible to increase the top energy by cycling the momentum of the stored beams between 450 GeV/c and some lower momentum (100 GeV/c) keeping the overall power dissipation at the same level as in normal DC Collider mode. After successful tests in summer 1984 a dedicated physics run of the pulsed Collider took place in March 1985, in which data were collected at $\sqrt{s} = 900$ GeV and 200 GeV.

During the pulsed Collider run a UA5 trigger was set up so as to accept highly asymmetric events of the diffractive type $p\bar{p} \rightarrow$ pX together with (more symmetric) non single-diffractive events. According to the above mass limit $M^2/s \leq 0.05$ the higher pulsed Collider energy corresponds to masses of the diffractive system $M \leq 200$ GeV. The following results are based on 500 (400) fully reconstructed asymmetric events at 900 (200) GeV and 25000 events recorded with a symmetric trigger. These data have already been used to measure the rise of the inelastic $p\bar{p}$ cross-section between 200 GeV and 900 GeV [12]. In this paper we present results for the single-diffractive (SD) cross-section at these two Collider energies. From a measurement of the relative rates of the asymmetric and symmetric triggers we may deduce the ratio of the single-diffractive to the inelastic cross-section. Using our previous data on the inelastic cross-section we thus calculate σ_{SD}.

By exploiting the large geometrical acceptance of the streamer chamber detector the pseudorapidity distribution[2] of diffractive events can be derived. In lower energy data it is rather difficult to make a clear distinction between the different models for the decay modes of diffractively produced systems. Fireball-type models [13,14] predict a spread of the decay products in rapidity space independent of the mass of the diffractive state, whereas in multiperipheral-type models [15,16] a width growing with mass is predicted. The considerable increase of collision energy at the Collider and hence the production of large diffractive masses allows us to distinguish unambigously between these two models.

---

[1] A peaking of the form $d\sigma/d(M^2/s) \simeq (M^2/s)^{-1}$ implies $d\sigma/dx \simeq 1/(1 - x_F)$ since $M^2/s \simeq (1 - x_F)$.

[2] The pseudorapidity η is defined as $\eta = -\ln\tan\frac{\Theta}{2}$, where Θ is the c.m. production angle. The minimum scattering angle at which we can detect charged tracks in the streamer chambers is 0.7^0, corresponding to a maximum pseudorapidity of 5.

Experimental details and the event generators used in our simulation programs are described in section II. Results for pseudorapidity distributions of single-diffractive interactions and the decay properties of diffractive states are presented in section III and the cross-section calculation is treated in section IV.

II. Details on data collection and event simulation

The UA5 detector consists of two large (6m x 1.25m x 0.5m) streamer chambers placed above and below the SPS beam pipe. The geometrical acceptance of the detector is about 95 % for $|\eta| \leq 3$ falling to zero at $|\eta| = 5$. Each chamber is viewed by 3 cameras, each recording a stereoscopic pair of views which allows a 3-dimensional reconstruction of the events. The methods by which streamer chamber tracks are measured, reconstructed and associated with primary and secondary vertices are explained in [17].

Triggering is achieved with two sets of scintillator hodoscopes placed at each end of the streamer chambers. The large solid angle covered ($2 \leq |\eta| \leq 5.6$) and the good time resolution allowed an efficient selection of beam-beam interactions and at the same time an effective suppression of background events due to beam-gas interactions. Details of the trigger can be found in [18].

A basic aim of the UA5 experiment is the detection of a large fraction of all inelastic events. This is achieved by running two different triggers in parallel. A symmetric (i.e. 2-arm) trigger requiring at least one hit of a charged particle in each hodoscope side is very efficient for non single-diffractive (NSD) events. A single arm (i.e. 1-arm) trigger in which hits are required in only one set of the hodoscopes selects highly asymmetric events,[1] for example single-diffractive (SD) events of the type $p\bar{p} \rightarrow pX$, where the recoil proton escapes detection and the fragments of X are largely confined to one hemisphere.

The sample of events recorded has to be examined to remove beam-gas interactions and showers induced by particles scattered out of the circulating bunches. In the case of 2-arm triggers the signature of beam-beam events is clear enough to distinguish background by scanning the film. For 1-arm triggers a scan provides a first rejection of obvious background and the remaining pictures are measured and more restrictive vertex cuts are applied. More details on the methods used to determine the fraction of beam-beam interactions in the data sample can be found in [12].

The observed 1-arm trigger sample is corrected for acceptance losses and contamination by non single-diffractive events using a Monte-Carlo (MC) method. Two different event generators are used to describe NSD and SD particle production. Produced particles are tracked through the whole detector geometry allowing for secondary interactions and scattering. A comparison between tracks generated and those observed in the chamber volume yields an efficiency ϵ as a function of pseudorapidity η, which is used to compute true pseudorapidity distributions from observed ones. We now describe briefly both event generators pointing out the relevant model uncertainties. The influence of these uncertainties on the results presented will be discussed below. Further details on our event simulation are given in [19].

The NSD generator has been tuned to reproduce accurately the main features of non-diffractive multiparticle production at Collider energies. In essence, a set of 'clusters' is generated, distributed according to p_t-limited phase space, and leading particles are situated at the ends of the rapidity chain. The charged particle multiplicity distribution is input from data. For the present study the crucial point is to estimate the number of NSD events satisfying the 1-arm trigger. There are the two main categories of events which give single-arm triggers.

[1] This single arm trigger is susceptible to beam-gas background having the same time structure as genuine beam-beam interactions. As the proton bunch was an order of magnitude more intense than the antiproton bunch, only data of the $\bar{p}$ diffractive type could be recorded with reasonably large fractions of beam-beam interactions in the data sample.

a) Events of very low multiplicity, where by chance no particle happens to hit one of the trigger arms. The simulation of this category should be reliable. The multiplicity distribution is taken directly from data. The production of particles in clusters, rather than individual production is important, since it leads to bigger forward-backward fluctuations of multiplicity, and the cluster parameters in the model are chosen to reproduce correlation data [19,20].

b) Events where the leading particle has $|x_F| > 0.95$ will be kinematically like SD events and will therefore tend to be asymmetric and give single-arm triggers. Data from FNAL and ISR [21-23] show a roughly uniform distribution in x_F for baryons, but the region $|x_F| > 0.95$ is of course dominated by the SD peak, and the form of the underlying NSD contribution is not clear. Our standard version of the NSD event generator imposes a $1\text{-}|x_F|$ form in this region (after ref [3]), while other possibilities such as a flatter distribution are also considered below as sources of systematic error in our measurements.

In the case of the SD event generator measurements from lower energy data (see for example the review of ref [3]) and latest results from the UA4 collaboration observing SD particle production at $\sqrt{s} = 546$ GeV [24] are incorporated into the model. In particular a $\frac{s}{M^2}$ form of the invariant cross-section, an exponential dependence of the cross-section on the four-momentum transfer t of the form $\frac{d\sigma}{dt} = \exp(-bt)$ with $b = 7\ GeV^{-2}$, and a range of diffractive masses M extending from a low mass cut-off $M_p + M_\pi = 1.08$ GeV to a maximum allowed by the coherence limit $\frac{M^2}{s} \leq 0.05$ are used. In general all parametrisations in the SD event generator follow the indications from the latest Collider data [25] that a diffractive system of mass M has similar features to an 'ordinary' $p\bar{p}$ interaction at an c.m. energy of M. The average transverse momentum $< p_T >$ of the decayproducts of the diffractive state affects the rapidity distribution of produced particles and influences the trigger efficiencies. Both the UA4 results [25] and our data (see below) favour a p_T-limited multiperipheral-type model, rather than an isotropic 'fireball' decay, and thus this uncertainty may be eliminated. The trigger efficiency for SD events is quite insensitive to the t-distribution, and so the assumed mass distribution $(1/M^2)$ is the main systematic uncertainty. In particular, our detector is not sensitive to the low mass (resonance) region, and the UA4 data are not accurate enough to define the M^2 behaviour here. The possible systematic error arising from changes in the low mass region is considered below.

III. Pseudorapidity distributions

The rapidity of a particle with energy E and longitudinal momentum p_L is defined as

$$y = 1/2 \ln(E + p_L)/(E - p_L) \tag{3-1}$$

which gives approximately for the pseudorapidity of the centre of mass of a diffractive state of mass M

$$\eta_M = \ln(\sqrt{s}/M) \tag{3-2}$$

The decay products of M are distributed in rapidity around the central value η_M, the width of this distribution depending on the decay mechanism. The particles produced in isotropic decays (N_0 particles in total) are uniformly distributed in the rest frame of the diffractive state ($dN/d\Omega = const$), which leads after the shift to the c.m. system of the initial collision to a pseudorapidity distribution of the form

$$dN/d\eta \; = \; 2N_0/\cosh^2(\eta - \eta_M) \tag{3-3}$$

This distribution has roughly a gaussian shape having a half width at half maximum (HWHM) $\Delta\eta$ independent of the mass of the diffractive state

$$\Delta\eta(\text{isotropic}) = 0.88 \tag{3-4}$$

whereas in multiperipheral models the width $\Delta\eta$(HWHM) of the distribution grows with increasing mass like

$$\Delta\eta(\text{multiperipheral}) \simeq \ln(M/ < \mu >) \tag{3-5}$$

where $\mu = \sqrt{p_T^2 + m^2}$ denotes the transverse mass of the particles into which the diffractive state decays (mainly pions). These different situations are illustrated in figure 1a. Our observed rapidity distribution of SD events is an average of such distributions for single events over all masses accepted by the 1-arm trigger. As the cross-section falls like $1/M^2$ one expects to observe roughly a triangular shaped pseudorapidity distribution, the width of this triangle depending on the decay kinematics as indicated in figure 1b.

To compare the observed 1-arm data with model predictions one has to consider that NSD events may also satisfy the 1-arm trigger. Figure 2 indicates how the inelastic cross-section divides into the NSD and SD parts and, as a result of our simulations at $\sqrt{s} = 900$ GeV, the fraction accepted by each trigger.

About 50 % (60%) of all single-diffractive events are accepted by the 1-arm trigger and give at least one track of 10 cm length in the streamer chambers at $\sqrt{s}$ = 900 (200) GeV. Figure 3 shows the efficiencies for each trigger for SD events as a function of their mass. We have chosen a logarithmic scale for the diffractive mass as in this presentation SD events (from a $1/M^2$ distribution) form a uniform distribution and hence the trigger efficiency is proportional to the area under the efficiency curve. Events with small masses have few charged particles produced with high rapidities, thus often missing the trigger counters, or have no tracks within the streamer chamber acceptance. For large masses particles are also produced in the opposite hemisphere and some events satisfy the 2-arm trigger.

Figure 4 shows the observed pseudorapidity distribution of charged particles in 1-arm triggers at 900 (4a) and 200 GeV (4b) in comparison with our model predictions. The contamination from NSD events, marked as a shaded area in figure 4, is rather small in the case of the 900 GeV data; the ratio of SD events to NSD events is calculated from the simulation to be about 5.5:1, whereas at 200 GeV the ratio is about 1:1. In both cases, the sum of the NSD- and SD-Monte Carlo simulations is normalized to the number of events in the data.[1]

[1]The ratio of the SD and NSD cross-sections depends on the precise model assumptions, as described in section IV. In all cases of figures 4 and 5 the relative normalization of the SD and NSD components is correctly determined using the formulae of section IV. In figure 4 we only show the NSD contamination for p_t-limited decay of diffractive states. In the case of isotropic decays the NSD contamination would be sligthly larger.

The simulation agrees well with the data in the case of p_T-limited decay of the diffractive state, whereas the simulations comprising an isotropic decay are too narrow and show too many tracks within the acceptance region of the streamer chambers to describe the data.

The favouring of p_T-limited decays of diffractive states becomes even more evident if one looks at the distribution of the standard deviation $\sigma_\eta^{\rm obs}$ of the observed particles around the observed centre $< \eta >_{obs}$, i.e.

$$\sigma_\eta^{\rm obs} = \sqrt{\frac{1}{n_{obs}} \sum_{i=1}^{n_{obs}} (\eta_i - < \eta >_{obs})^2} \qquad (3\text{–}6)$$

Figure 5 shows the distribution of $\sigma_\eta^{\rm obs}$ for both energies in comparison with the model predictions, which should show a significant difference between the two decay schemes (compare equations (3-4) and (3-5)). As there is a correlation between the mass of the diffractive system and the number of observed charged tracks, we have divided the data into 3 different ranges of the number of observed particles n_{obs}. The distribution of σ_η^{obs} for the lowest band of observed multiplicities (predominantly low masses) does not allow us to distinguish between isotropic or p_T-limited decays. This reflects the difficulty in distinguishing between the two decay modes at lower c.m. energies, as larger masses were not produced. As n_{obs} increases, the discrepancy between the data and the prediction assuming isotropic decay becomes evident, whereas in the case of p_T limited decays we get a good description of the data for all multiplicities and at both energies.

From the observed pseudorapidity distribution of 1-arm triggers we are able to derive the distribution for single-diffractive events only. To do this we first subtract the contribution of NSD events as predicted by our Monte Carlo assuming a $1 - |x_F|$ shape of the leading particle x_F-distribution. We then correct the remaining SD events for acceptance and trigger efficiency. Figure 6 shows the resulting corrected SD distributions at both Collider energies, with our SD Monte Carlo predictions for comparison. The description of the data is very good in the case of the 900 GeV events, whereas at 200 GeV the corrections for NSD contamination are very large (compare figure 4) and the description of the remaining SD-data by the simulation (taking all model parameters as at 900 GeV) is less good. The errors shown in figure 6a and 6b are statistical only, a subtraction of more tracks due to a larger NSD-contamination in the case of a flatter x_F-distribution of the leading particles would move all data points systematically to lower values in less good agreement with our simulations.

As there is no magnetic field in our detector we cannot measure the momenta of particles directly. However the shape of the simulated pseudorapidity distribution of diffractive events is sensitive to the transverse momenta of the decay products. For larger average transverse momenta, more charged tracks of low mass diffractive states become visible in the acceptance region of the chambers. It is possible to deduce a rough value for the average transverse momentum of all charged decay products by comparing our data with the outcome of our simulations with different averages as input. The average transverse momentum of charged particles $< p_T >_{\rm ch}^{\rm SD}$ was varied in the simulations between 0.3 GeV/c and 0.7 GeV/c. We get the best description of the 900 GeV data for $< p_T >_{\rm ch}^{\rm SD} = 0.45$ GeV/c (solid curve in figure 6). From the 900 GeV distribution we conclude $< p_T >_{\rm ch}^{\rm SD} = (0.45 \pm 0.1)$ GeV/c at both Collider energies as a rough estimate within the framework of our model assumption of p_t-limited decay.

The mean number of charged particles, $< n_{ch} >$, is calculated by integrating the pseudorapidity distribution of figures 6. Since our MC simulations provide a good description of the data within the acceptance region of our detector, we have used them to extrapolate over the whole kinematic region[1]. The resulting values for the charged decay products of diffractive states (i.e. not including the recoil particle of the interaction) are:

[1] i.e. we use

$$< n_{ch}^{SD} > = < n_{|\eta|\leq 4.5}^{\rm data} > \cdot \frac{< n_{{\rm all}\ \eta}^{\rm MC} >}{< n_{|\eta|\leq 4.5}^{\rm MC} >}$$

$$\langle n_{ch}^{SD} \rangle = 6.5 \pm 1.0 \quad \text{at 900 GeV}$$

and

$$\langle n_{ch}^{SD} \rangle = 4.1 \pm 1.1 \quad \text{at 200 GeV}$$

The errors include statistical errors ($\sim$ 10% at each energy) combined with a systematic contribution estimated by making the following changes to the event generators:

i) In the NSD model the x_F distribution of the leading baryon in the region $|x_F| > 0.95$ was changed from a (1-$|x_F|$) form to a flatter distribution, which can be parametrized as $d\sigma/dx_F \propto (1\text{-}\frac{|x_F|}{2})$ for $|x_F| > 0.95$. This yields a larger NSD contamination in the 1-arm triggers and represents the largest change we can make while remaining compatible with the data of figures 4 and 6.

ii) To account for the uncertainties in the shape of the mass distribution of low mass diffractive events we enhanced the low mass region (M $\leq$ 2.5 GeV) by 50% [26] and studied the effect on our results. Such events are almost never detected in this experiment. This change has the effect of reducing $\langle n_{ch}^{SD} \rangle$ and of increasing the single-diffractive cross-section σ_{SD}.

iii) The average transverse momentum of the diffractive decay products $\langle p_T \rangle$ was varied over the range which we find to be compatible with our data, 0.35 GeV/c to 0.55 GeV/c.

In this section we have presented results which unambigously favour p_T-limited fragmentation of diffractive states. The average transverse momentum of the decay products of diffractive states is found to be similar to the value measured in non single-diffractive interactions. The mean number of observed particles (which we observe as an average over all diffractive masses) agrees well with our simulations assuming a rise of the average number of particles as a power of the diffractive mass. These results support the evidence reported earlier by the UA4 collaboration [24], that the fragmentation of a diffractive state with mass M is very similar to a hadronic collision at a c.m. energy of $\sqrt{s}$ = M.

IV. Cross-Sections

IV.1 Experimental method

Our measurement of σ_{SD} is based on a measurement of the corresponding interaction rate over the whole run time. The event rate $\dot{N}$ for a given trigger at any time t is related to the luminosity $\mathcal{L}(t)$ and the triggering cross-sections, σ_1 and σ_2 , through

$$\dot{N}_i(t) = \sigma_i \, \mathcal{L}(t) \qquad (4\text{-}1)$$

i=1,2 for 1-arm or 2-arm triggers respectively.

The method used to determine the total interaction rates $\dot{N}_1$ and $\dot{N}_2$ is described in detail in [12] so we include only a short summary here:

To determine the ratio r of the two triggering cross-sections ($r = \sigma_1 / \sigma_2$), we write for the interaction rates

$$\dot{N}_1 = \frac{2 \, f_1 \, N_1}{\Delta t} \qquad (4\text{-}2)$$

$$\dot{N}_2 = \frac{f_2 \, N_2}{\Delta t} \qquad (4\text{-}3)$$

where N_1 and N_2 are the number of 1-arm and 2-arm triggers during the active time Δt. The factors f_1 and f_2 denote the fraction of beam-beam interactions in the total number of triggers found by examination of the corresponding streamer chamber pictures. The extra factor of 2 in equation (4-2) arises from the fact that we were able to use only one of the two possible 1-arm trigger configurations (see chapter II).

Putting in all measured quantities N_1, N_2, f_1, f_2, Δt [12] we get:

$$r = 0.111 \pm 0.009 \qquad \text{at } \sqrt{s} = 900 \text{ GeV}$$

$$r = 0.153 \pm 0.015 \qquad \text{at } \sqrt{s} = 200 \text{ GeV}$$

the quoted errors being statistical.

Single-diffractive and non single-diffractive particle production contribute in different proportions to the two trigger cross-sections. Hence one may write in obvious notation for the trigger efficiencies ϵ :

$$\begin{pmatrix} \sigma_1 \\ \sigma_2 \end{pmatrix} = \begin{pmatrix} \epsilon_1^{SD} & \epsilon_1^{NSD} \\ \epsilon_2^{SD} & \epsilon_2^{NSD} \end{pmatrix} \begin{pmatrix} \sigma_{SD} \\ \sigma_{NSD} \end{pmatrix} \tag{4-4}$$

Solving equation (4-4) for σ_{SD} /σ_{NSD} one finds:

$$R = \frac{\sigma_{SD}}{\sigma_{NSD}} = \frac{r \cdot \epsilon_2^{NSD} - \epsilon_1^{NSD}}{\epsilon_1^{SD} - r \cdot \epsilon_2^{SD}} \tag{4-5}$$

The trigger efficiencies ϵ in equation (4-5) were determined using the simulations described in section II. From the results described in section III we assume a p_t-limited decay of diffractive states, removing the largest systematic uncertainty in the simulations. Table 1 shows values of the 1-arm trigger efficiencies resulting from different model assumptions. Those marked with an asterisk we have used for the cross-section calculations, while the others have been used to calculate the systematic uncertainties as discussed at the end of chapter III.

IV.2 Single-Diffractive Cross-Section

The UA5 collaboration has already published a measurement of the ratio of the inelastic cross-sections at $\sqrt{s} = 200$ and 900 GeV [12]. This measurement yields a value $\sigma_{inel}(900) = (50.3 \pm 0.4 \pm 1.0)$ mb (first error statistical, second systematic) from the interpolated value $\sigma_{inel}(200) = (41.8 \pm 0.6)$ mb. Taking both numbers as input we can calculate an absolute cross-section σ_{SD} using

$$\sigma_{SD} = \sigma_{inel} \cdot \frac{\sigma_{SD}}{\sigma_{inel}} = \sigma_{inel} \cdot \left(\frac{R}{R+1}\right) \tag{4-6}$$

From our measured values of r and the trigger efficiencies discussed in the last paragraph we calculate using equation (4-5):

$$R = 0.180 \pm 0.014 \pm 0.029 \qquad \text{at } \sqrt{s} = 900 \text{ GeV}$$

$$R = 0.132 \pm 0.016 \pm 0.024 \qquad \text{at } \sqrt{s} = 200 \text{ GeV}$$

and with the above numbers for the inelastic cross-sections

$$\sigma_{SD} = (7.8 \pm 0.5 \pm 1.1) \text{ mb} \quad \text{at } \sqrt{s} = 900 \text{ GeV}$$

$$\sigma_{SD} = (4.8 \pm 0.5 \pm 0.8) \text{ mb} \quad \text{at } \sqrt{s} = 200 \text{ GeV}$$

the first error being statistical and the second systematic.

Figure 7 shows these results together with a large number of measurements of the single-diffractive cross-section over a wide range of c.m.energies, where different experimental techniques were used to extract single-diffractive events. We have included measurements of the SD cross-section for different definitions of the M^2/s high mass limit and for various experimental methods of extracting the single-diffractive sample [27], resulting in partially inconsistent results at the same energies. For example, at ISR energies the measurements for $M^2/s \leq 0.06$ from one experiment give lower cross sections than for $M^2/s \leq 0.05$ from another experiment at about the same energy, indicating the difficulties of measurements of this cross-section. It appears that the single-diffractive cross-section increases only

slightly with energy, in contrast with the tendency, suggested by the ISR data [28], that the the SD cross-section is a constant fraction of the total $p\bar{p}$ cross-section ($\sigma_{SD} = 0.17\ \sigma_{tot}$). This would yield a single-diffractive cross-section of about 11 mb at 900 GeV and 9 mb at 200 GeV, both of which are clearly ruled out by the Collider measurements.

Four measurements of the single-diffractive cross-section at collider energies are shown in figure 7. Our own measurement at $\sqrt{s} = 546$ GeV based on 1-arm trigger and 2-arm trigger data recorded in 1982 has larger systematic uncertainties, as the relative normalization of the trigger cross-sections σ_1 and σ_2 (needed to determine r in equation 4-5) was less well known since the triggers were enabled at different run times. This uncertainty was completely removed at the pulsed collider run in 1985 where changes to the trigger hardware allowed data taking with both triggers in parallel. Furthermore, the quality of our measurements was better at the higher pulsed Collider energy. At 900 GeV the contamination from NSD events, and hence the effect of different model assumptions to correct for this, is much smaller (see also the shaded areas in figures 4 and 5). In any case, an underestimate of the NSD contamination yields too large a SD cross-section. In this light, the somewhat larger cross-section at $\sqrt{s}$ =546 GeV reported by the UA4 collaboration (although compatible with our measurement at 546 GeV and 900 GeV) is possibly due to NSD events which happen to have a large rapidity gap and hence survive their rapidity gap cut defining the 'single-diffractive' sample. (compare [24]). All collider measurements, together with the values at highest ISR energies are in fact compatible with the single-diffractive cross-section being constant with a value between 5 and 8 mb.

IV.3 Double-Diffractive Cross-Section

We have attempted to estimate the cross-section for double-diffractive particle production. Therefore we used the formalism of section IV.1 expanding all equations to a third unknown cross-section σ_{DD}, by separating σ_{NSD} into a non diffractive component σ_{ND} and the double-diffractive component σ_{DD}.

$$\begin{pmatrix} \sigma_1 \\ \sigma_2 \\ \sigma_{2'} \end{pmatrix} = \begin{pmatrix} \epsilon_1^{SD} & \epsilon_1^{ND} & \epsilon_1^{DD} \\ \epsilon_2^{SD} & \epsilon_2^{ND} & \epsilon_2^{DD} \\ \epsilon_{2'}^{SD} & \epsilon_{2'}^{ND} & \epsilon_{2'}^{DD} \end{pmatrix} \begin{pmatrix} \sigma_{SD} \\ \sigma_{ND} \\ \sigma_{DD} \end{pmatrix} \qquad (4\text{–}7)$$

The neccessary third measured input cross-section $\sigma_{2'}$ we derive from our 2-arm trigger data σ_2 applying extra cuts which are chosen to enhance the double-diffractive component in the remaining data.

We used two different methods to define $\sigma_{2'}$, which independently lead to consistent results for σ_{DD} within errors:

1) The cross-section $\sigma_{2'}$ may be defined imposing an extra cut on the 2-arm trigger data requiring no charged track within a central pseudorapidity region $|\eta| \leq \eta_c$, with $\eta_c \simeq 2.5$ typically. This cut tends to select double diffractive events with moderate masses at each vertex. If a cluster has too small a mass then it may give no tracks in the streamer chambers (the acceptance falls steeply for $|\eta| \geq 4$), while large masses will yield particles in the central region. To give a rough idea of the effect of the cut, we note that the minimum rapidity of a decay product of a diffractive state is given by $\eta_{min} \sim \ln(< \mu > \sqrt{s}/M^2)$ (fig 1a). Thus, the requirement $2.5 \leq |\eta_{min}| \leq 4$ corresponds to a range of $3 \leq M \leq 6$ GeV/c^2 for the mass of both diffractive clusters.

2) Alternatively we may define $\sigma_{2'}$ by requiring no charged tracks in one c.m. hemisphere. Such an asymmetric event satisfying a 2-arm trigger is likely to be a double-diffractive event where one of the masses is very small, giving no tracks in the streamer chambers, but nevertheless producing a particle which hits the trigger counters. The low mass cluster therefore has $4 \leq |\eta_{min}| \leq 5.6$, or $1.2 \leq M_1 \leq 3$ GeV/c^2, whilst the other cluster, which produces tracks in the chamber acceptance, all in one hemisphere, has $0 \leq |\eta_{min}| \leq 4$, or $3 \leq M_2 \leq 20$ GeV/c^2.

For both methods all trigger efficiencies ϵ in equation (4-7) were determined using the MC simulations described in chapter II. To simulate DD events we used the SD event generator to simulate both

diffractive systems independently which were then combined to form a DD event. The central gap cut in method 1 was varied between $\pm$ 1 and $\pm$3 units in pseudorapidity and the veto on tracks in one hemisphere in method 2 was extended into part of the opposite hemisphere. For these cuts a typical efficiency for a DD event is 10%, whereas only about 1% of non-diffractive events satisfy the cuts. The fraction of DD events in all inelastic $p\bar{p}$ interactions is then found at both Collider energies to be 0.09 ± 0.04 for method 1 and 0.07 ± 0.04 for method 2. The errors quoted are statistical uncertainties and include the dependence of the results on the cuts.

From this we conclude:

$$\frac{\sigma_{DD}}{\sigma_{inel}} = 0.08 \pm 0.05$$

with the maximum limits of the results above as overall error. With the values for σ_{inel} from section IV.2 we finally obtain

$$\sigma_{DD} = (4.0 \pm 2.5) \text{ mb at 900 GeV}$$

$$\sigma_{DD} = (3.5 \pm 2.2) \text{ mb at 200 GeV}$$

One may compare these results with calculations assuming factorization of diffractive vertices. If factorization holds for the double-diffractive cross-section it may be written [3]:

$$\sigma_{DD} = \frac{\sigma_{SD}^2}{4\sigma_{el}} \cdot \frac{b_{SD}^2}{b_{el}\, b_{DD}} \qquad (4\text{–}8)$$

with the following relation between the slope parameters b of the exponential dependence of all three diffractive cross-sections on the 4-momentum transfer t ($d\sigma/dt = a \cdot e^{b \cdot t}$).

$$b_{DD} = 2b_{SD} - b_{el}$$

In the Collider energy range data for σ_{el}, b_{el} and b_{SD} are only available at $\sqrt{s} = 546$ GeV [29,30], so we compare our result with calculations based on 546 GeV measurements. Taking $\sigma_{el} = (13.6 \pm 0.6)$ mb, $b_{el} = 15$ GeV^{-2}, $b_{SD} = 8 \pm 1$ GeV^{-2} and $\sigma_{SD} = (7 \pm 1)$ mb formula (4-8) yields a value for σ_{DD} between 2 and 4 mb in approximate agreement with our measurements.

V. Summary

The successful operation of the pulsed Collider has made it possible to observe diffractive states up to very large masses ($M \leq 200$ GeV/c^2) with the UA5 detector. The cross section for single-diffractive particle production was found to be $(7.8 \pm 0.5 \pm 1.1)$ mb at 900 GeV and $(4.8 \pm 0.5 \pm 0.8)$ mb at 200 GeV c.m. energy (first error statistical, second systematic). The shape of the pseudorapidity distribution of the decay products of diffractive states clearly rules out isotropic decays, instead favouring a p_t limited fragmentation with an average of the transverse momenta of the decay products of diffractive states of (0.45 ± 0.1) GeV/c. The mean number of charged particles is found to be 6.5 ± 1.0 at 900 GeV and 4.1 ± 1.1 at 200 GeV. The cross-section estimates for double-diffractive particle production of (4.0 ± 2.5) mb at 900 GeV and (3.5 ± 2.0) mb at 200 GeV c.m. energy (combined statistical and systematic error) give results compatible with expectations based on factorization of diffractive vertices.

Acknowledgements. *We acknowledge with thanks the financial support of the Brussels group by the National Foundation for Fundamental Research and the Inter-University Institute for Nuclear Sciences, of the Bonn group by the Bundesministerium für Wissenschaft und Forschung, of the Cambridge group by the UK Science and Engineering Research Council, and of the Stockholm group by the Swedish Natural Science Research Council. Last, but not least, we acknowledge the contribution of the engineers, scanning and measuring staff of all our laboratories.*

References

[1] E.L. Feinberg and I.Pomeranchuk, Suppl. Nuovo Cimento **4** (1956) 652.

[2] M.L. Good and W.D. Walker, Phys. Rev. **120** (1960) 1855.

[3] K. Goulianos, Phys. Rep. **101** (1983) 169-219.

[4] S.N. Ganguli and D.P. Roy, Phys. Rep. **67** (1980) 201-395.

[5] R.G. Roberts and D.P. Roy, Nucl. Phys. **B77** (1977) 240.

[6] A.B. Kaidalov, Phys. Lett. **116B** (1982) 459.
A.B. Kaidalov and K.A. Ter-Martirosyan,Phys. Lett. **117B** (1982) 246, and ref. therein

[7] A. Capella and J. Tran Than Van, Z. Phys. **C18** (1985), 85.
A. Capella, J. Tran Than Van and J. Kaplan, Nucl. Phys. **B105** (1976) 333.

[8] C. Pajares, A. Varias and P. Yepers, Z. Phys. **C19** (1983) 89.

[9] A. Donnachie and P.V. Landshoff, Nucl. Phys. **B244** (1984) 322.

[10] L. van Hove and K. Fiałkowski, Nucl. Phys. **B107** (1976) 211.

[11] J.G. Rushbrooke, CERN Preprint, CERN/EP 82-6 (1982).
UA5 Collaboration, CERN/SPSC/82-75, SPSC/P184, 15-October 1982.

[12] G.J. Alner et al., 'Antiproton-Proton Cross Sections
at 200 GeV and 900 GeV C.M. Energy', submitted to Zeitschrift für Physik C

[13] R. Hwa, Phys. Rev. Lett. **26** (1971) 1143.

[14] M. Jacob and R. Slansky, Phys. Rev. **D5** (1972) 1847.

[15] D. Amati et al., Nuovo Cimento **26** (1962) 896.

[16] G. Fox, CALT68-43 (1968).

[17] UA5 Collaboration, in preparation for Physics Report

[18] H. Schmickler, A. Drees, 'UA5- Triggersystem' CERN/EP/SCE-R703T-UA5/T 84-16

[19] G.J. Alner et al., 'The UA5 High Energy $p\bar{p}$ Simulation Program'
to be submitted to Nuclear Instruments and Methods

[20] K. Alpgård et al., Phys. Lett. **123B**, (1983) 361.

[21] C.P. Ward et al., Nucl. Phys. **B153** (1979) 299.

[22] F.C. Erne et al., Phys. Lett. **49B** (1974) 356.

[23] F. Palmonari, Lecture given at the Europhysics Study Conference on Jet Structure from Quark and Lepton Interactions, Erice, Sicily, 12-17 Sept. 1982 and references [7-9] therein.

[24] V. Palladino (UA4), 'Diffraction Dissociation at the SPS Collider' Invited Talk at the Workshop on Elastic and Diffractive Scattering 3-6 June 1985, Chateau de Blois, France

[25] D. Bernard et al., Phys. Lett. **166B** (1986) 459.

[26] S. Belforte and K. Goulianos (1984),
'Monte Carlo Study of Single-Diffractive Trigger and Luminosity Monitor', CDF note No. 257.

[27] M.G. Albrow et al., Nucl. Phys. **B108** (1976) 1.
J. Whitmore et al., Phys. Rep. **C10** (1974) 273.
J.W. Chapman et al., Phys. Rev. Lett. **32** (1974) 257.
S. Barish et al., Phys. Rev. **D9**, (1974) 2689.
H. Bialkowska et al., Nucl. Phys. **B110** (1976) 300.
J. Schamberger et al., Phys. Rev. Lett. **34** (1975) 121.
J.C.M. Armitage et al., Nucl. Phys. **B194** (1982) 365.
A. Breakstone et al., Phys. Rev. **30** (1984) 528.

[28] J.C.M. Armitage et al., Nucl. Phys. **B194** (1982) 365.

[29] M. Bozzo et al., Phys. Lett. **147B** (1984) 392.

[30] M. Bozzo et al., Phys. Lett. **147B** (1984) 385.

Figure Captions

Fig. 1a) 'Decay' width of diffractive states in pseudorapidity for isotropic decays and p_t-limited decays.
1b) Expected shape of the pseudorapidity distribution of single-diffractive events, if distributions as in figure 1a are overlayed assuming a $1/M^2$ mass distribution.

Fig. 2) The relations between physical subprocesses of the total $p\bar{p}$ cross-section and the two triggers of the UA5 experiment. Numbers are shown for $\sqrt{s} = 900$ GeV.

Fig. 3) Trigger efficiencies as a function of the mass of the diffractive state at the Collider energies 900 GeV (a) and 200 GeV (b).

Fig. 4) Observed pseudorapidity distribution of charged particles recorded with the 1-arm trigger at $\sqrt{s} = 900$ GeV (4a) and $\sqrt{s} = 200$ GeV (4b). The sum of the SD- and NSD-MC simulations assuming p_t-limited decay or isotropic decay of diffractive states are normalized to the number of events in the data. The NSD contamination is shown only for the case of p_t-limited decays. In case of isotropic decays the contamination would be slightly larger.

Fig. 5) Observed distribution of the standard deviation σ_η^{obs} arround the observed centre $< \eta^{obs} >$ in 3 bands of observed multiplicities. The figures are used to distinguish between isotropic or p_t-limited decay of diffractive states (see text). Figure 5a shows the distribution for 900 GeV assuming p_t-limited decay, 5b for 900 GeV isotropic decay, 5c for 200 GeV p_t-limited decay and 5d for 200 GeV isotropic decay. Before subdivision into different bands of observed multiplicities the sum of the SD- and NSD-MC simulations was normalized to the number of events in the data.

Fig. 6) Corrected pseudorapidity distribution for single-diffractive events at the Collider energies 900 GeV (a) and 200 GeV (b) in comparison to MC simulations assuming average transverse momenta of the decay products of diffractive states in the range 0.35 GeV/c to 0.55 GeV/c.

Fig. 7) The cross section for single-diffractive dissociation σ_{SD} as a function of the c.m. energy. Data from refs [24,27] and this experiment.

Table Caption

Table 1) List of trigger efficiencies under different model assumptions. The asterisk denotes the values used for the final cross-section determination.

Table 1

NSD-MC 900 GeV	ϵ_1^{NSD}	ϵ_2^{NSD}
$\star(1-\lvert x_F\rvert)$	0.017 ± 0.001	0.968 ± 0.010
$(1-\lvert x_F\rvert/2)$	0.030 ± 0.002	0.956 ± 0.018
SD-MC 900 GeV	ϵ_1^{SD}	ϵ_2^{SD}
$< p_T >_{ch} = 0.55$ GeV/c	0.52 ± 0.03	0.10 ± 0.01
$\star < p_T >_{ch} = 0.45$ GeV/c	0.50 ± 0.01	0.12 ± 0.004
$< p_T >_{ch} = 0.35$ GeV/c	0.48 ± 0.02	0.16 ± 0.01
$< p_T >_{ch} = 0.45$ GeV/c masses below 2.5 GeV/c^2 enhanced by 50%	0.46 ± 0.01	0.111 ± 0.003
NSD-MC 200 GeV	ϵ_1^{NSD}	ϵ_2^{NSD}
$\star(1-\lvert x_F\rvert)$	0.063 ± 0.002	0.927 ± 0.012
$(1-\lvert x_F\rvert/2)$	0.075 ± 0.004	0.915 ± 0.017
SD-MC 200 GeV	ϵ_1^{SD}	ϵ_2^{SD}
$< p_T >_{ch} = 0.55$ GeV/c	0.61 ± 0.02	0.040 ± 0.004
$\star < p_T >_{ch} = 0.45$ GeV/c	0.60 ± 0.02	0.048 ± 0.004
$< p_T >_{ch} = 0.35$ GeV/c	0.60 ± 0.02	0.051 ± 0.004
$< p_T >_{ch} = 0.45$ GeV/c masses below 2.5 GeV/c^2 enhanced by 50%	0.55 ± 0.02	0.044 ± 0.004

figure 1a

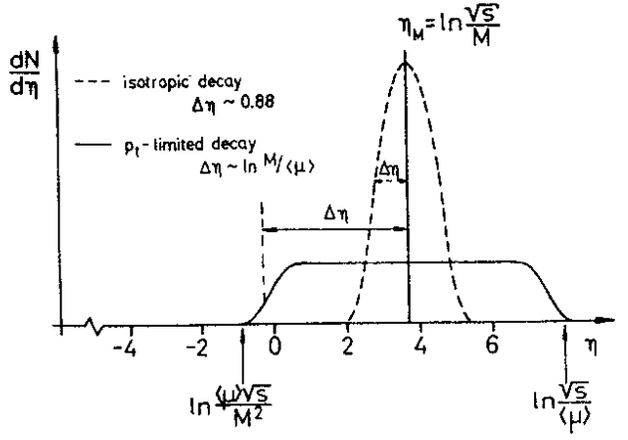

figure 1b

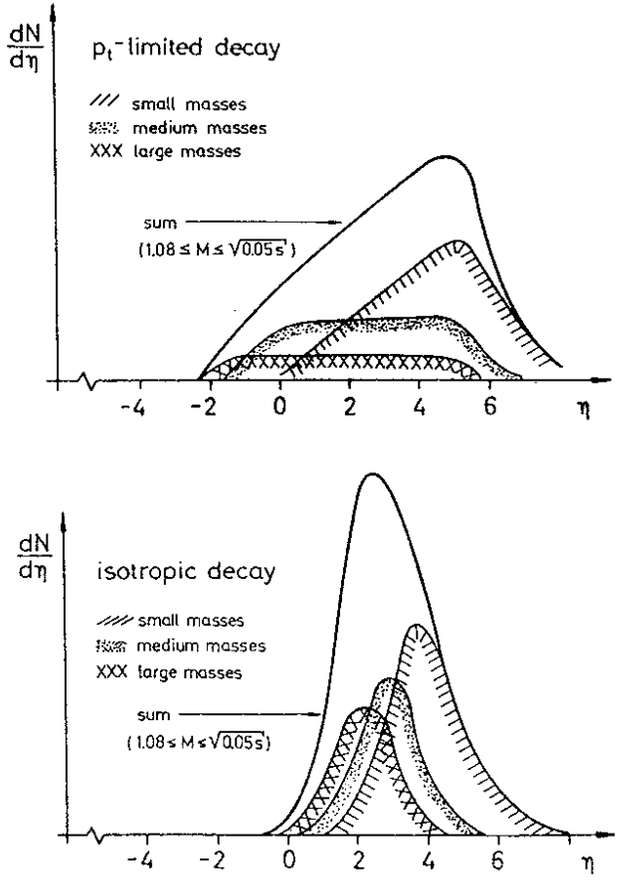

figure 2

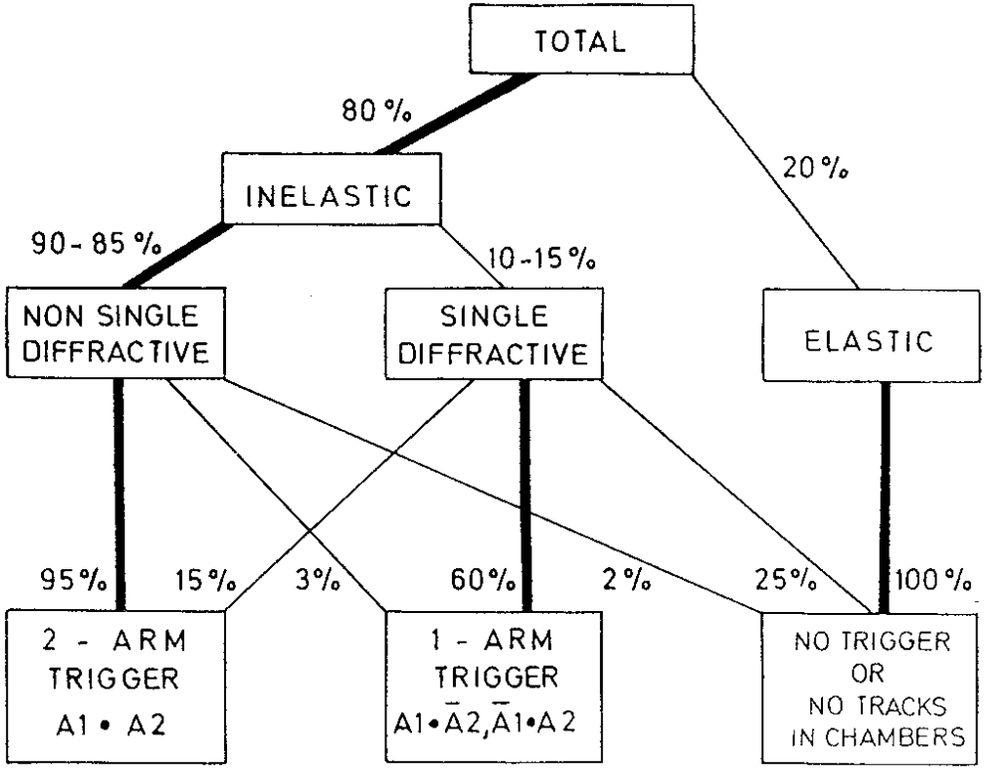

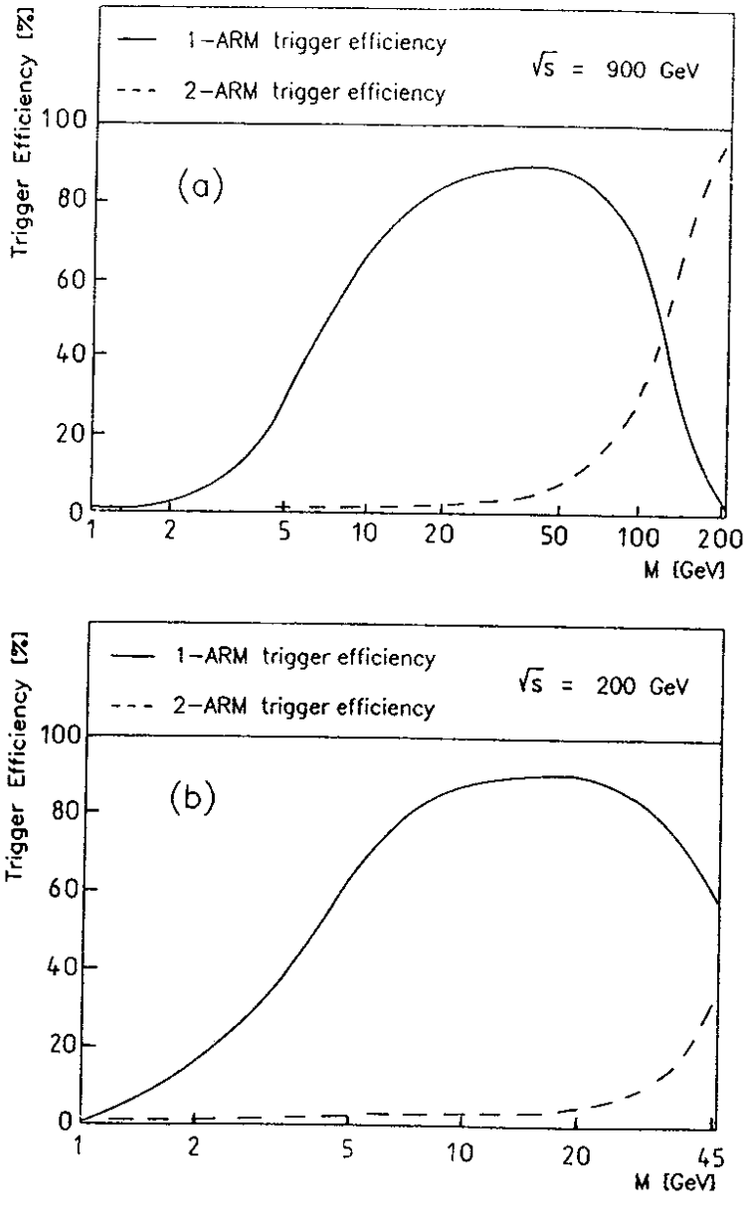

figure 3

figure 4

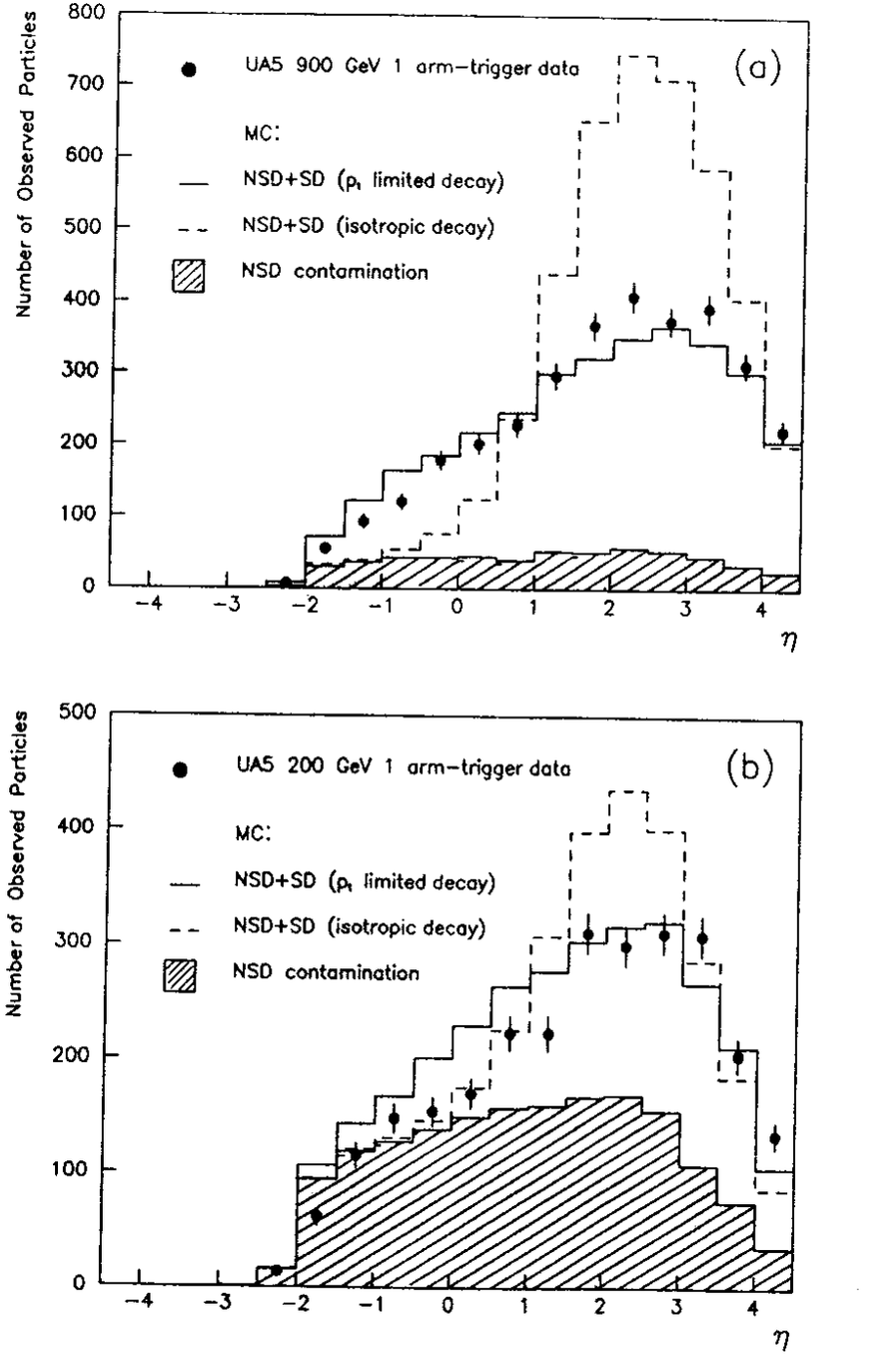

figure 5

figure 5

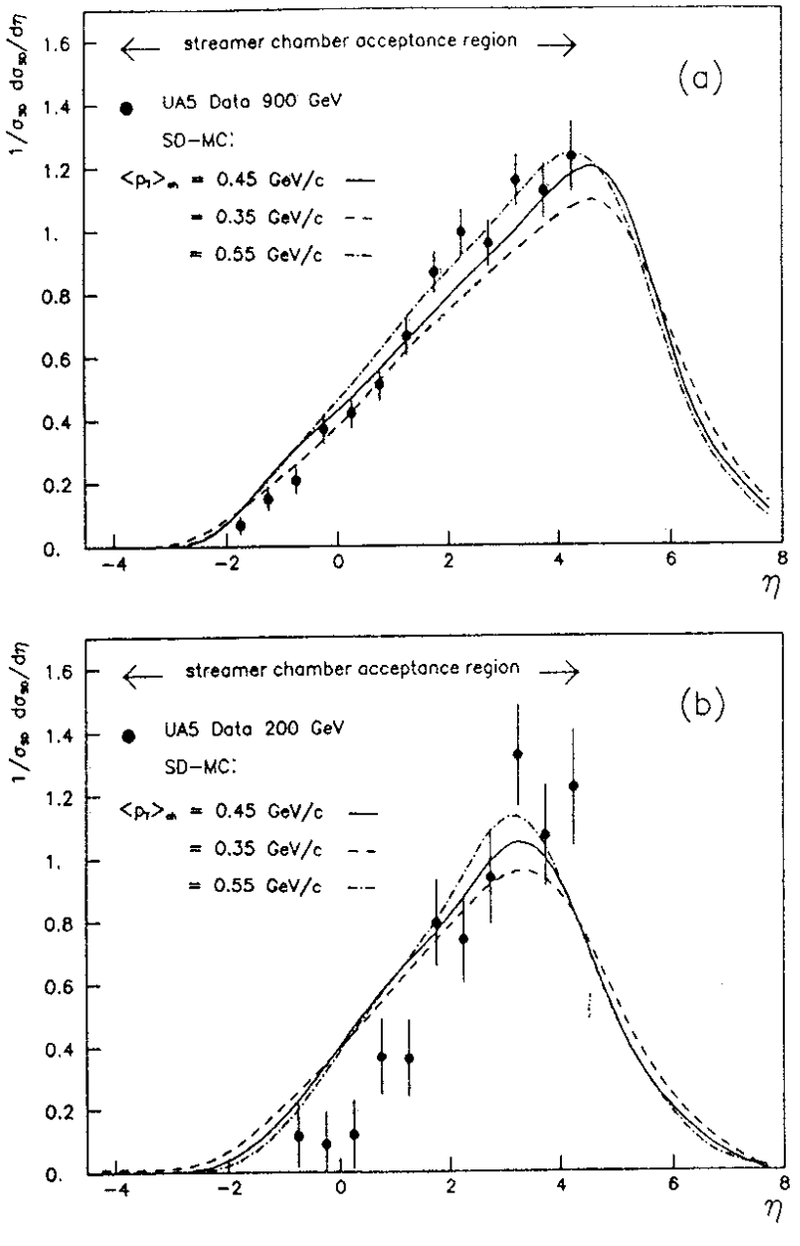

figure 6

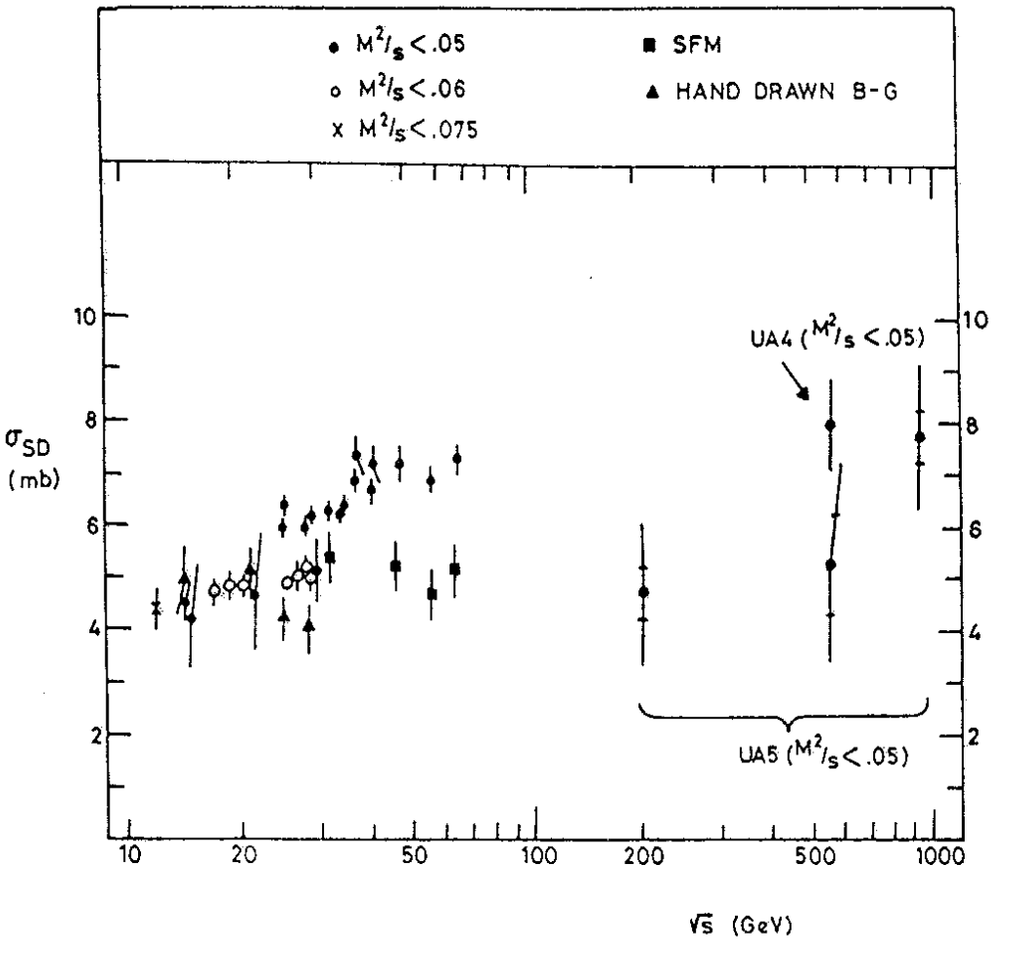

figure 7